Thermal modeling of PMMA microfluidic separation chips

Y. Zhu and A. Bui

CSIRO Manufacturing and Infrastructure Technology
PO Box 56, Highett, Melbourne, Victoria 3190, AUSTRALIA
yonggang.zhu@csiro.au
anh.bui@csiro.au

ABSTRACT

Understanding the thermal performance of electrokinetically driven microfluidic chips is important since Joule heating could raise the temperature significantly and affect the separation efficiency. In this paper, we present the thermal modeling of polymethylmethacrylate (PMMA) polymer separation chips using computational methods with a whole-chip approach. Both a simple cross and a multichannel separation chip were used in the study. The numerical study was carried out using the multiphysics CFD package CFD-Ace+. The heat generation was essentially uniform and the subsequent temperature increase was uniform along the channel(s) except for regions near the liquid ports. For the simple cross chip, the Joule heating effect was negligible for the studied conditions. For the multichannel separation chip, the heat generation was much higher and the maximum temperature could reach over 80°C at an electric field of 68kV/m one minute after the separation starts. For moderate electric field (~45kV/m), the heating effect was also significant and it is suggested that active heat dissipation measures be used for polymer chips to alleviate excessive temperature rise.

Keywords: microfluidics, separation, Joule heating, thermal modeling, CFD

1 INTRODUCTION

Microfluidic devices have attracted more and more interest over the last decade due to the advantages of high efficiency and reduction in analysis time, reagent consumption and cost in comparison with conventional laboratory bench-top analysis. One of the key components of these devices is the microfluidic chip which may be used for sampling, mixing, separation and detection. The commonly used technique for manipulating analytes on chip is electrokinetics, i.e. an electric field is applied to induce electroosmotic flow and electrophoretic motion of particles in microchannels. However, this can produce Joule heating which affects the electroosmotic flow, analyte diffusion, and ultimately the efficiency and reproducibility of the separation [1].

The Joule heating problem has been investigated extensively since the last decades or so [1-11] . Most of the work in the past have focused on the glass capillaries. Only a few studies have been carried out to investigate the effect of Joule heating on microfluidic chips, especially those made of polymer materials [7,9]. Further, the current studies have mostly used computational fluid dynamics (CFD) in conjunction with some in-channel temperature measurements [12-15]. Zhu et al. [15] provided the first 'whole-chip' experimental data to validate the computational results obtained for a simple cross separation chip. On the basis of the validation, this study will extend the modeling to more complicated chip design. In particular, we will model the thermal performance of a multichannel separation chip designed for 2-d separation using isoelectric focusing (IEF) and capillary electrophoresis (CE) techniques [18-21]. The results will be used to determine the optimal designs for such separation chips and the effect on molecule transport in microchannels.

2 MODELING DETAILS

2.1 Microfluidic chips

The thermal performance was investigated for two microfluidic chips, one with a simple cross geometry and the other with eight separation channels, both were made of polymethylmethylacrylate (PMMA). The simple cross separation chip was purchased from the Microfluidic ChipShop GmbH in Germany. The chip has a simple T-channel (see Figure 1) and the port-to-port length of the separation channels is 87.8 mm while the sampling channel has a length of 10 mm and is located 6 mm form the left port. The separation channels run through the middle of the chip. For the simple cross chip, the shape of the cross section of the channel is trapezoidal with a height of 20 μm, top width of 70 μm and bottom width of 42 μm. The chip is 95 mm long and 16 mm wide. The total thickness of the chip is 2 mm and the thickness of the cover lid for the channel is 175 μm. The multichannel chip was fabricated in-house using laser ablation technique. The microchannel pattern was designed using a CAD package and micromachined onto the PMMA substrate using a chrome-on-quartz mask and an excimer laser projection system (Exitech Series 8000) at Minifab Pty Ltd, Scoresby, Victoria 3179, Australia. The micromachined channels were then cleaned and bonded to a polymer thin film as a capping layer using a lamination process. Four liquid ports

were drilled using a minidrill machine prior to the capping process. The cross section of the channel is nearly rectangular with sizes of 50 μm × 35μm.

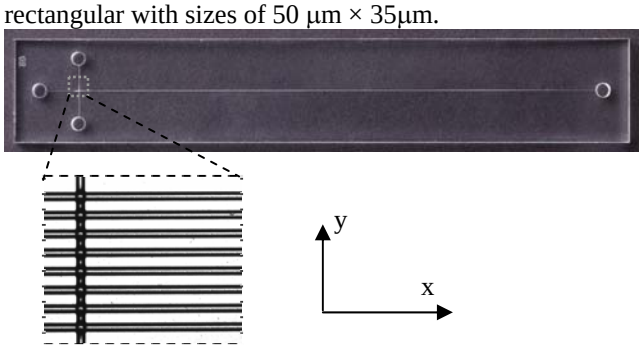

Figure 1 A picture of the whole chip with a detailed image of the intersection area and the coordinate system. The origin is located at the centre of the left liquid port.

2.2 Materials

The PMMA material has a density of 1190 kg/m3, a specific heat *Cp* of 1450 J/(kg.K) and a thermal conductivity of k = 0.18. The density of the solution is 1006 kg/m^3, specific heat 4180 J/(kg.K), thermal conductivity k 0.61+0.0012(T-T_0), dynamic viscosity μ 2.761×10^{-6} exp(1713/T) and dielectric constant ε is 305.7 exp(-T/219) [7]. The electrical conductivity σ of the solution was assumed to have the same temperature dependence as water and, given its value at the room temperature equal to 0.129S/m, the general expression for the solution electrical conductivity was assumed to be 0.129[(1+0.02(T-T_0)] S/m.

3 COMPUTATION DETAILS

3.1 Fluid flow and heat transfer equations

The flow in the micro channels was described by the system of the Navier-Stokes equations:

$$\frac{\partial(\rho v)}{\partial t} + \nabla(\rho v \otimes v) = -\nabla p + \nabla[\mu(T)\cdot\nabla v] + \rho_e E \ , \quad (1)$$

where $\boldsymbol{E}$ is the externally applied electric field (defined as $\boldsymbol{E}$=-$\nabla\phi$, with ϕ being the electric potential), ρ is the density of the fluid, v is the velocity vector, p is the pressure, μ is the viscosity of the fluids and ρ_e is the charge density of the fluid. The heat generation in the channels is governed by the Joule heating which was added to the energy conservation equation as follows:

$$\frac{\partial \rho C_p T}{\partial t} + \nabla(\rho v C_p T) = \nabla[k(T)\cdot\nabla T] + \sigma(T)E\cdot E \ , \quad (2)$$

where T represents temperature. In the solid regions, a heat diffusion equation was solved which is similar to the above equation with the convective and Joule-heating terms omitted.

Since the thickness of the EDL was very small compared to the channel cross-sectional size, the EDL was not directly modeled and the effect of the EDL on the flow was described by a moving-wall boundary condition. The boundary speed is calculated using [16, 17]:

$$V = -\frac{\varepsilon(T)\varepsilon_o\zeta(T)}{\mu(T)}E \ , \quad (3)$$

where ε_0 is the permittivity of vacuum and ζ is the zeta potential. The published data of zeta potential for PMMA substrate showed large discrepancy [18]. For the current simulations, a value of –0.03V was used in all simulations.

3.2 Numerical methods

The computational fluid dynamics (CFD) software CFD-ACE+ was utilized for the modeling of the flow and heat transfer in the whole microfluidic chip which included both fluid and solid regions. The computational domain for the microfluidic chip is shown in Figure 2. The total number of control volumes was 23,325 with higher grid resolution implemented around the microchannels. The external heat transfer boundary condition was applied for the chip outer surfaces with the ambient temperature assumed to be 293 K and the heat transfer coefficient between the chip surfaces and the surrounding air assumed to be 10 W/(m^2.K). The simulated chip operating conditions are listed in Table 1. Both the single and multichannel chips were modeled using these conditions. The fluid channels were described as one-dimensional filaments which were embedded in the chip. The flow in the channels was assumed to have a flat velocity profile (one-dimensional). The previous study [15] revealed that the temperature distributions in a simple cross chip obtained from the CFD modeling agreed reasonably well with experimental data, thus providing a validation of the assumption.

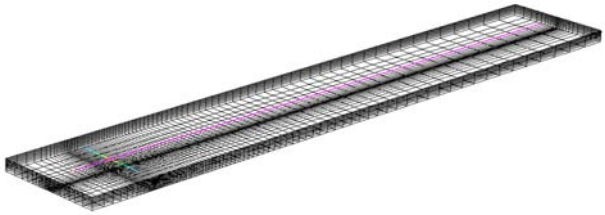

Figure 2 The computation domain.

Case	Sampling Channel	Separation Channel
1	20kV/m	23kV/m
2	40kV/m	45kV/m
3	60kV/m	68kV/m

Table 1 Operating conditions used for modeling.

4 RESULTS

Figure 3 shows typical temperature fields on the bottom surface of the multichannel chip for Case 2 at times of 20, 22, 30, 60 and 120s, respectively. A cross sectional view of the field is shown in Figure 4. The switching from sampling to separation occurred at 20s. The figures show the initial heating up of the sampling channel and the following heating up of the long separation channels. Due to the thin

cover plate, more heat was dissipated through bottom and higher temperature on the bottom surface was predicted. Similar temperatures distribution patterns were predicted for the single channel chip [15] although the temperature increase was much higher in the multichannel chip.

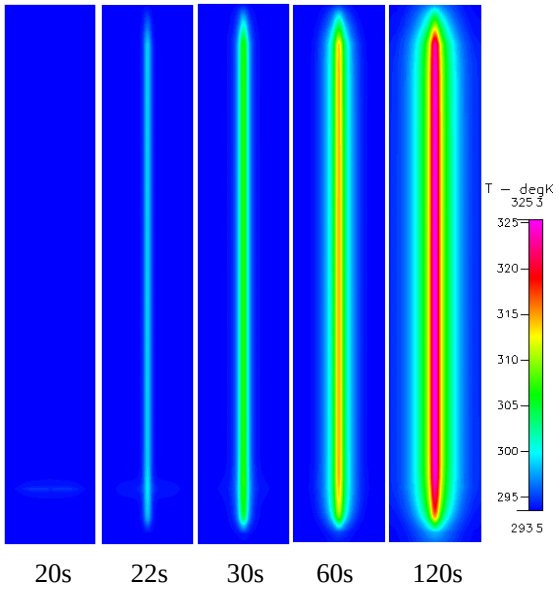

Figure 3 Temperature fields on the bottom surface. Case 2.

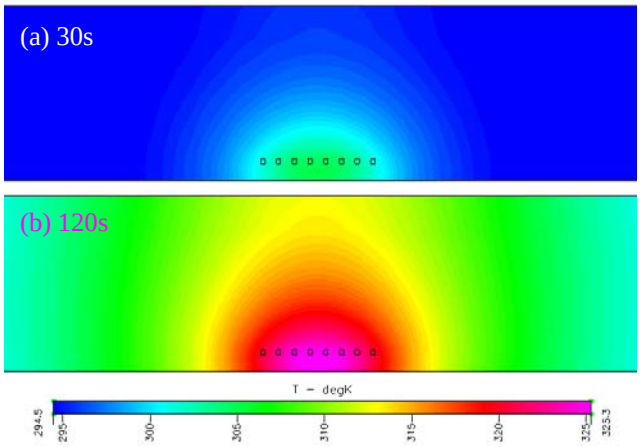

Figure 4 Temperature fields across the multichannel chip at 30s (a) and 120s (b) from separation, respectively. Case 2. Only central region is shown for clarity. The axis to axis distance between channels is 150μm.

The detailed temperature distributions along the axis of a central long channel and a crossing line located on the channel plane for Case 2 are shown in Figure 5. The temperature of the chip was seen to increase with time and have the maximum value along the channel centreline. The heating was nearly uniform along the channel except for regions near the liquid ports (and the chip edges). The small local temperature peaking at x =10mm was due to the heat generated from the sampling step. The uniformity of the heat distribution along the channel indicates the small effect of the heat convection due to the fluid flow on the heat transfer in the chip.

In the cross section planes, the temperature distributions were non-uniform with hot spots expectedly observed around the micro-channels. The maximum temperature increase was predicted to be around 20°C at 60s from the start of separation, significantly higher than that (1.5°C) obtained for the single channel chip operating at similar conditions [15]. Figure 4 also shows that for multichannel chips the temperatures in channels at the edge is smaller than those at the centre and the difference increase with the electric fields. For example, at an electric field of 45kV/m, the difference was 5°C whereas at 68kV/m the difference could be as high as 20°C.

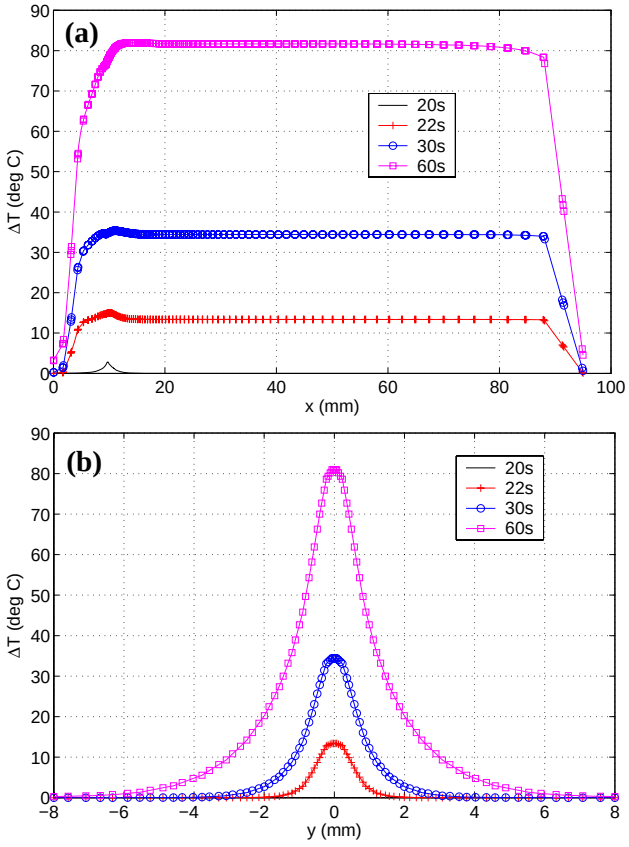

Figure 5 Computed temperature distributions of the multichannel chip along a channel axis (a) and a crossing line at x=80mm (b). Case 2. All data are at the channel centre level.

The temperature responses for different operating conditions are shown in Figure 6 and Figure **7** for the two chips, respectively. Also shown in Figure 7 are the simulation results assuming the multichannel chip had a glass substrate. As expected, the higher thermal conductivity of glass allowed heat to be conductivity more effectively and therefore a much lower temperature increase.

For the single channel chip, the centreline temperature increased with time and the maximum temperature increase was around 0.4, 1.6 and 9°C, respectively, for 23, 45, and 68 kV/m electric fields after 2 minutes from the start of separation. Such a small increase implies that the Joule heating effect was negligible for the single channel chip operating at the studied conditions. However, for the multi channel chip, the increases after 1 minute from the start of separation were 4, 20 and 81°C, respectively, for the three electric fields, which were much higher than those for the single chip. Therefore, the effect of Joule heating must be taken into account in the analysis of the transport of molecules through the microchannels. For the chips operating with high electric fields, some active heat dissipation measures is recommended to alleviate excessive temperature rise.

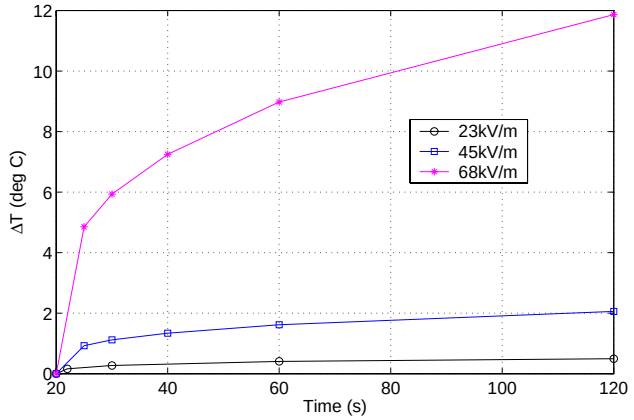

Figure 6 Temperature increase as a function of time for different operating conditions. Single channel chip.

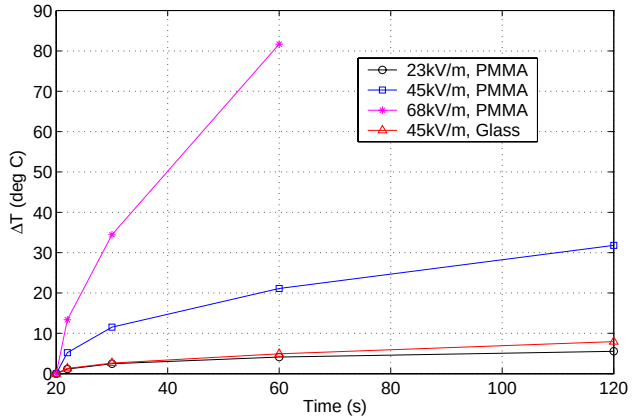

Figure 7 Temperature increase as a function of time for different operating conditions. Multi channel chip.

5 CONCLUSIONS

The thermal performance of PMMA microfluidic separation chips was investigated using the multiphysics CFD package CFD-Ace+ and a whole-chip approach. Both a simple cross and a multichannel separation chip were used in the study. It was found that the heating was approximately uniform in the separation channels except for regions near the liquid ports. Higher temperature increase was predicted along the centerlines of the channels and on the bottom surface of the chip. For the simple cross chip, the Joule heating effect was negligible for the solution used and an electric field up to 68kV/m. For the eight channel separation chip, the heat generation was much higher and the maximum temperature could reach over 80°C one minute after the beginning of the separation phase at an applied electric field of 68kV/m. For moderate electric fields (~45kV/m), the heating effect was still significant and it is suggested that some active heat dissipation measures must be used for polymer chips to prevent excessive temperature rise. For multichannel separation chips or chips with large aspect channels, non-uniformity of temperature field should be taken into account.

REFERENCES

1. Rathore, A. S., *J. Chromat. A*, **1037**, 431-443, 2004.
2. Ermakov, S.V., S.C. Jacobson, and J.M. Ramsey, *Anal. Chem*., **70**, 4494-4504, 1998.
3. Rathore, A.S., K.J. Reynolds & L.A. Colón, *Electrophoresis*, **23**, 2918, 2002.
4. Swinney K. & D.J. Bornhop. *Electrophoresis*, **23**, 613, 2002.
5. Erickson, D., D. Sinton and D. Li, *Lab Chip*. **3**, 141, 2003.
6. Chen G., U. Tallarek, A. Seidel-Morgenstern and Y. Zhang,. *J. Chromat. A*, **1044**, 287–294, 2004.
7. Horiuchi K. & P. Dutta, *Int. J. Heat Mass Trans.*, **47**, 3085-3095, 2004.
8. Matsumoto, H., N. Komatsubara, C. Kuroda, N. Tajima, E. Shinohara and H. Suzuki, *Chem. Eng. J.*, **101**, 347, 2004.
9. Petersen, N. J., R. P. H. Nikolajsen, K. B. Mogensen and J. P. Kutter, *Electrophoresis*, **25**, 253–269, 2004.
10. Xuan, X. D. Sinton, and D. Li, *Int. J. Heat Mass Transfer*, **47**, 3145-3157, 2004a.
11. Xuan, X., B. Xu, D. Sinton & D. Li, *Lab Chip*. **4**, 230, 2004b.
12. Lacey, M. E., A. G. Webb and J. V. Sweedler, *Anal. Chem.*, **72**, 4991-4998, 2000.
13. Ross, D. M. Gaitan, and L. E. Locascio, *Anal. Chem*., **73**, 4117-4123, 2001.
14. Benninger, R.K.P., Y. Koç, O. Hofmann, J. Requejo-Isidro, M.A.A. Neil, P.M.W. French, & A.J. deMello. Quantitative 3D-Mapping of Fluidic Temperatures within Microchannel Networks using Fluorescence Lifetime Imaging. Private communication.
15. Zhu, Y., S. Nahavandi, A. Bui and K. Petkovic-Duran, Proceedings of SPIE, 6036, 2005.
16. Oddy, M. H., J. G. Santiago, and J. C. Mikkelsen, *Anal. Chem*. 2001, 73, 5822-5832
17. Probstein, R. F., Physicochemical hydrodynamics, 2nd edition, John Wiley and Sons, 2003.
18. B.J. Kirby & E.F. Hasselbrink, Electrophoresis **25**, 203, 2004.
19. J.C. Sanders, Z. Huang and James P. Landers, *Lab on a Chip*, **1**, 167–172, 2001.
20. H Beckeryx, K Lowackz and A Manzyk, *J. Micromech. Microeng.* **8** 24–28, 1998.
21. X. Chen, H. Wu, C.Mao, and G.M. Whitesides, *Anal. Chem.* **74**, 1772-1778, 2002.